An Advanced System for the Automatic Classification of Multitemporal SAR Images

Lorenzo Bruzzone, *Senior Member, IEEE*, Mattia Marconcini, Urs Wegmüller, *Senior Member, IEEE*, and Andreas Wiesmann, *Member, IEEE*

***Abstract*—A novel system for the classification of multitemporal synthetic aperture radar (SAR) images is presented. It has been developed by integrating an analysis of the multitemporal SAR signal physics with a pattern recognition approach. The system is made up of a feature-extraction module and a neural-network classifier, as well as a set of standard preprocessing procedures. The feature-extraction module derives a set of features from a series of multitemporal SAR images. These features are based on the concepts of long-term coherence and backscattering temporal variability and have been defined according to an analysis of the multitemporal SAR signal behavior in the presence of different land-cover classes. The neural-network classifier (which is based on a radial basis function neural architecture) properly exploits the multitemporal features for producing accurate land-cover maps. Thanks to the effectiveness of the extracted features, the number of measures that can be provided as input to the classifier is significantly smaller than the number of available multitemporal images. This reduces the complexity of the neural architecture (and consequently increases the generalization capabilities of the classifier) and relaxes the requirements relating to the number of training patterns to be used for classifier learning. Experimental results (obtained on a multitemporal series of European Remote Sensing 1 satellite SAR images) confirm the effectiveness of the proposed system, which exhibits both high classification accuracy and good stability versus parameter settings. These results also point out that properly integrating a pattern recognition procedure (based on machine learning) with an accurate feature extraction phase (based on the SAR sensor physics understanding) represents an effective approach to SAR data analysis.**

***Index Terms*—Backscattering temporal variability, classification, feature extraction, image analysis, long-term coherence, multiclass problems, multitemporal synthetic aperture radar (SAR) images, neural networks.**

I. Introduction

SYNTHETIC aperture radar (SAR) sensors are becoming more and more important in remote sensing applications. Their importance is based on the properties of SAR signals, the most significant of which being: 1) the sensitivity of the backscattering coefficient to target geometry and permittivity; 2) the coherent nature of the electromagnetic pulse that permits interferometry; and 3) the fact that the measures are almost completely independent of atmospheric conditions and solar illumination. While the first two factors above are related to the specific information contained in SAR signals, the third emphasizes the great robustness and wide applicability of SAR techniques in real problems. For these reasons, SAR sensors can play an important role in several application domains dealing with the production of land-cover maps, especially in cases in which remote sensing with optical sensors fails due to the unavailability of cloud-free data.

Nevertheless, there are understandable reasons for the limited use of SAR data for land-cover classification, such as the special SAR imaging geometry (which results in the undesired presence of shadow, layover, and foreshortening phenomena in the images), the complicated scatter process, and the presence of speckle noise [1]. For the above reasons, it is generally difficult to obtain high classification accuracies if only one single-channel single-polarization SAR image is considered, even if advanced classification procedures are used [2], [3]. In order to mitigate these problems, classification of SAR data is usually applied to more complex datasets. In particular, the most typical operational frameworks are the following: 1) use of multichannel, fully polarimetric images [4]–[7]; 2) fusion between data acquired by different SAR sensors [8], [9] or between SAR data and multispectral images [10]–[12]; and 3) use of series of multitemporal images acquired on the same geographic area at different dates [13], [14]. Despite the fact that the multichannel fully polarimetric data may increase the separability of land-cover classes in the feature space, at present their use is limited to airborne remote sensing systems, given the technical problems that prevent the development of multichannel fully polarimetric SAR sensors on satellites. If proper classification techniques are used [11], [12], the integration between SAR data and multispectral images can result in accurate land-cover maps. This depends on the complementary information provided by active microwave and passive optical sensors. However, in operational applications, multispectral data are often not available (e.g., depending on cloud-covers). In this context, in recent years, the remote sensing community has become increasingly interested in the use of multitemporal SAR data for the production of land-cover maps [13], [14]. On the one hand, with multitemporal images, the SNR of the SAR data can be improved (without significantly degrading the spatial resolution of the images) thanks to multitemporal filtering approaches; on the other hand, multitemporal data allow to identify different land-cover classes by analyzing the temporal behavior of the backscattering coefficient (i.e., the "temporal

Manuscript received August 9, 2003; revised January 11, 2004. This work was supported by the European Space Agency (ESA) and the Italian Ministry of Education, University and Research (MIUR).

L. Bruzzone and M. Marconcini are with the Department of Information and Communication Technology, University of Trento, 38050, Povo, Trento, Italy (e-mail: lorenzo.bruzzone@ing.unitn.it).

U. Wegmüller and A. Wiesmann are with the Gamma Remote Sensing, CH-3074 Muri, Switzerland (e-mail: wegmuller@gamma-rs.ch).

Digital Object Identifier 10.1109/TGRS.2004.826821

signature" of a given pixel). For these reasons, multitemporal SAR images have become a relatively operational tool for classification problems involving few land-cover classes [15]–[17]. Nevertheless, at present, multitemporal SAR data are not yet operative in the solution of more complex multiclass problems.

For a proper exploitation of multitemporal SAR data in in multiclass classification problems, we need to develop a system based both on: 1) effective preprocessing and feature-extraction procedures and 2) an appropriate classification methodology that should take into account the peculiarities of currently available multitemporal SAR signals.

In the literature, the most important features used for the classification of multitemporal SAR data are the European Remote Sensing (ERS) 1/2 Tandem coherence and the Japanese Earth Resources (JERS) L-band SAR backscattering coefficient [16]–[22]. Unfortunately, these parameters are no longer available at present or in the near future. Currently used satellite-borne SAR sensors include ERS-2, Radarsat, and ENVISAT, all of which are repeat-track C-band SAR sensors and have interferometric capability. The repeat intervals are 35 days for ERS-2 and ENVISAT and 24 days for Radarsat. However, since very short repeat-pass intervals are unavailable with these sensors, nothing like ERS-1/2 Tandem coherence can be retrieved with them.

The selection of the classification algorithm is another critical issue in the classification of multitemporal SAR data. When standard features associated with the intensity or amplitude of single-date SAR signals are exploited , maximum-likelihood classifiers are commonly used [23]. However, when nonlinear features extracted from multitemporal images are considered, parametric classifiers become more difficult to use, as it is not possible to make reasonable assumptions on the distribution of derived multitemporal measures. In these cases, rule-based hierarchical thresholding classifiers have been proposed in the literature [14]. However, these classifiers do not allow to exploit the information of multitemporal features fully.

In this paper, we propose an advanced classification system for the analysis of multitemporal SAR data that addresses the aforementioned issues. The proposed system is made up of three main modules: 1) a preprocessing module; 2) a feature-extraction module to derive effective features from the original multitemporal SAR data; and 3) a classification module based on the use of a distribution-free neural classifier. The preprocessing module is based on a set of procedures commonly used in multitemporal SAR data processing. The feature-extraction module computes a reduced set of effective features from the multitemporal images. These features, which are based on the backscattering temporal variability of images and on long-term coherence (computed on images acquired 24–35 days apart, or multiples thereof), were derived by taking into account both the physics of the multitemporal signals and their behaviors in presence of different land-cover classes. This allows to avoid blind feature-extraction processes that do not take into account SAR data properties. The classification module is based on radial basis functions neural networks, which properly exploit the peculiarity of multitemporal features to produce accurate land-cover maps.

The main novelties of the proposed system consist of the following: 1) the integration of a reliable feature-extraction approach based on the physics of multitemporal SAR signals with an effective advanced pattern recognition approach that exploits a specific neural network architecture; 2) the joint use of backscattering temporal variability and long-term coherence features for solving a multiclass problem with multitemporal SAR data; 3) the application of a radial basis function neural classifier to multitemporal SAR data, which is characterized by good generalization capabilities and properly exploits the peculiarities of the two features above for producing accurate land-cover maps. It is worth noting that a relevant aspect of the proposed system is that the used features can be derived from the currently operating spaceborne SAR sensors.

The system has been tested on a multitemporal series of ERS-1 SAR images acquired on the area of Bern, Switzerland. Experimental results confirmed the effectiveness of the proposed approach.

The paper is organized in six sections. Section II deals with the problem formulation and briefly introduces the preprocessing procedures adopted in the proposed system. Section III presents the feature-extraction module, addressing the motivation and definition of the features developed in the proposed system, with an analytical description. Section IV describes the classification module, which is based on radial basis function neural networks. The experimental results are reported in Section V, and finally, Section VI contains a discussion and conclusions.

II. Problem Formulation and Preprocessing Techniques

A. Problem Formulation

Let us consider a series of M multitemporal complex SAR images acquired on the same geographic area at different times $t_i, i = 1, \ldots M$. Let C_i $(i = 1, \ldots, M)$ be the ith complex image of the considered temporal series. S_i $(i = 1, \ldots, M)$ is the corresponding preprocessed (i.e., coregistered and calibrated) complex image and I_i $(i = 1, \ldots, M)$ is the related intensity image. Let J_i $(i = 1, \ldots, M)$ be the ith image obtained by applying a multitemporal filtering to the entire set of M intensity images $I_1, \ldots, I_M$. The M preprocessed complex images $S_1, \ldots, S_M$ and the M temporally filtered images $J_1, \ldots, J_M$ are given as input to the feature-extraction block. Let $\bar{x}_p$ be the feature vector that represents the pth pattern in input to the classifier, and x_q $(q = 1, \ldots, Q)$ the qth component of the feature vector, which is derived from the feature-extraction block. Finally, let R be the number of land-cover classes in the considered classification problem. The block scheme of the proposed system with the above-defined notation is shown in Fig. 1.

Given the complexity of the automatic classification of SAR images, we focused the development of the proposed system on a specific challenging classification problem, which is very important from the application viewpoint. In particular, we considered a four-class problem aimed at discriminating forest, fields, urban, and water classes (it is worth noting that features capable of separating these classes are implicitly suitable to address simpler problems involving combinations of them, such as the im-

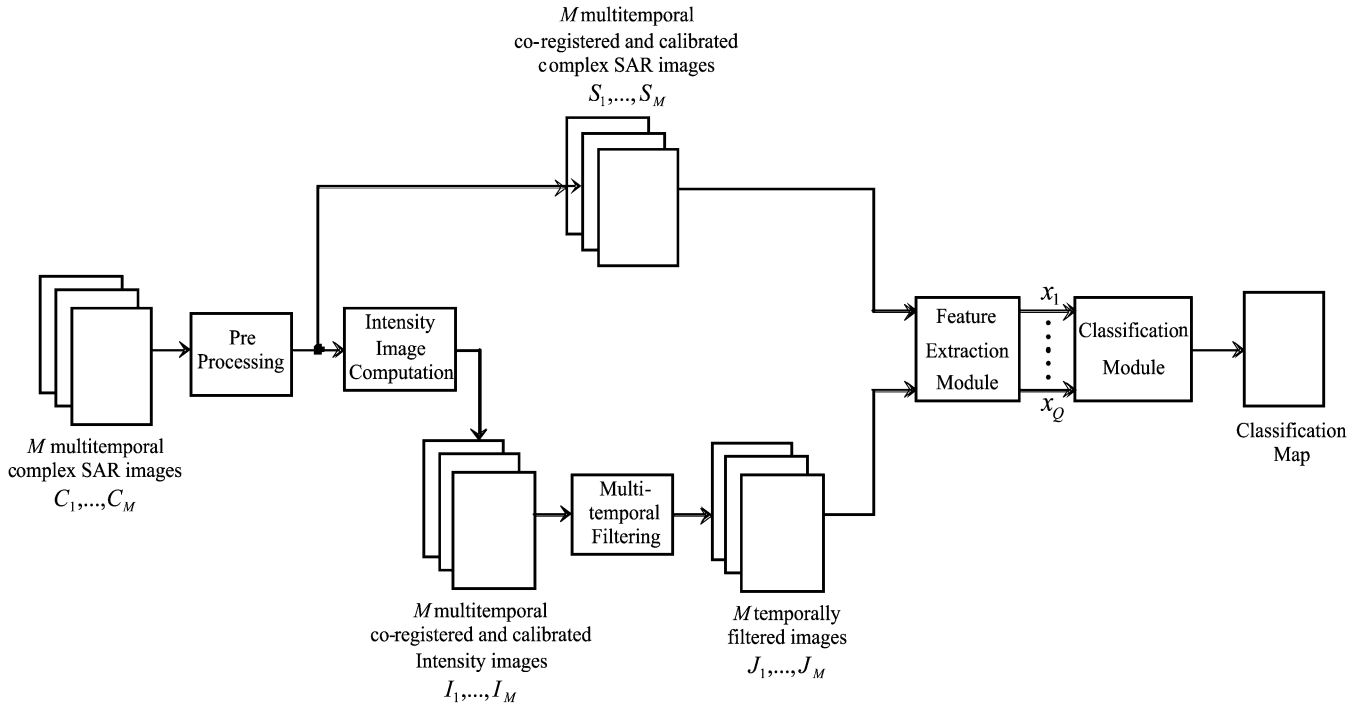

Fig. 1. Block scheme of the proposed system.

portant two-class forest against nonforest problem or the urban against nonurban problem). Nevertheless, the proposed system is general and can be easily extended to the discrimination of other classes, provided that multitemporal SAR images contain sufficient information for their separation. This condition depends on both the intrinsic availability of information about the classes investigated in the multitemporal SAR signal, and the number of temporal images considered [1].

B. Preprocessing Techniques

As stated in the introduction, the preprocessing techniques adopted in our system are the typical methods used in the literature for SAR data processing of multitemporal scenes (e.g., see [24]). In particular, the preprocessing module includes radiometric calibration and coregistration to a common geometry in range-Doppler. The radiometric calibration was conducted but without correcting for the effect of the local terrain slope on the pixel area. This is adequate, as the related correction factors remain the same across all images and therefore do not affect the backscatter temporal variability used in the classification. The image coregistration was done for the complex valued SLC data using automated algorithms designed for SAR interferometry, which assured accuracies better than 0.2 SLC pixels. Since these steps are carried out according to well-known methods, we refer the reader to the literature for further details on these aspects [1], [24]. In the following, we focus our attention on the adopted despeckling filtering technique, given its importance for SAR data classification.

In order to increase the SNR ratio of multilook SAR images, appropriate noise reduction processing schemes should be considered [25]. In the proposed system, this is done by applying temporal and spatial filtering to multitemporal images [26]. As

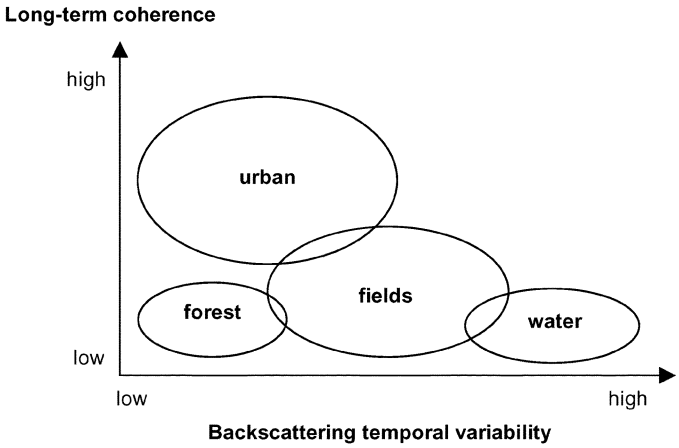

Fig. 2. Qualitative analysis of the distribution of the considered classes (i.e., forest, fields, water, and urban areas) in the backscattering temporal variability and long-term coherence feature space.

a starting point, we take the methodology for multitemporal C-band backscatter data proposed in [13]. Multitemporal filtering is applied to coregistered and calibrated images; the main aim of this process is to create a set of M speckle-reduced images by linearly combining the M registered intensity images I_i acquired on the same geographic area. The adopted filter function is the one described in [26], i.e.,

$$J_k = \frac{\sigma_k}{M} \sum_{i=1}^{M} \frac{I_i}{\sigma_i}, \qquad 1 \le k \le M \tag{1}$$

where J_k is the filtered output for the kth input image, and σ_k is the estimate of the local mean backscattering coefficient. σ_k is estimated from the data by averaging intensity values in a

TABLE I
ESTIMATORS FOR THE BACKSCATTER TEMPORAL VARIABILITY OF A REGISTERED MULTITEMPORAL DATASET OF M INTENSITY SAR IMAGES. $\sigma_{\max}$ AND $\sigma_{\min}$ ARE THE MAXIMUM AND MINIMUM BACKSCATTER VALUES OF THE M IMAGES AT THE GENERIC COORDINATES (x, y)

Backscattering Temporal Variability Estimator	Equation
Standard Deviation	$stdev = \sqrt{\frac{1}{M} \cdot \sum_{i=1}^{M} \sigma_i^2 - \sigma_{ave}^2}$
Normalized Standard Deviation	$\frac{stdev}{\sigma_{ave}} = \sqrt{\frac{1}{M} \cdot \sum_{i=1}^{M} \frac{\sigma_i^2}{\sigma_{ave}^2} - 1}$
Logarithmic Measure Based on Normalized Standard Deviation	$10 \cdot \log_{10}\left(\frac{stdev}{\sigma_{ave}} + 1\right)$
Saturation	$saturation = \frac{\sigma_{max} - \sigma_{min}}{\sigma_{max}}$
Standard Deviation of dB Values	$stdev = \sqrt{\frac{1}{M} \cdot \sum_{i=1}^{M} (10 \cdot \log_{10} \sigma_i)^2 - \left(\frac{1}{M} \cdot \sum_{i=1}^{M} 10 \cdot \log_{10} \sigma_i\right)^2}$
Maximum-Minimum Ratio in dB	$10 \cdot \log_{10}\left(\frac{\sigma_{\max}}{\sigma_{\min}}\right)$

local window around each pixel in each image. In our case, a Frost adaptive filter was chosen on account of its good trade-off between reliability of the local estimate and limited spatial degradation [27].

III. PROPOSED FEATURE EXTRACTION MODULE BASED ON BACKSCATTERING TEMPORAL VARIABILITY AND LONG-TERM COHERENCE

A. Background and Rationale of the Proposed Feature Set

A study on the features to be considered in the proposed system was carried out considering the peculiarities of the four-class problem addressed. In particular, the physics of both the multitemporal SAR signal and its interactions with the analyzed classes were studied also by considering previous results published in the literature. In this context, we can observe that the forest class can be discriminated based on the low temporal variability of the backscattering coefficient as compared to most other cover types [13]. Also the separation between forest and fields is good based on temporal variability (the temporal variability of fields is higher because of a stronger influence of soil moisture changes, vegetation growth, and cultivation phenology). Another class with low temporal variability is the urban class. Consequently, it seems appropriate to choose a feature based on the estimation of temporal variability from the considered time series of images.

In order to increase the effectiveness of the considered feature set, a second information source with complementary information should be extracted from the multitemporal data. A possibility could be to use the average backscattering coefficient as a second parameter. In fact, urban areas show very high backscatter values for several pixels. However, an analysis of the histogram of the temporal average of the backscattering coefficient on urban sites shows that its range of values is very wide and overlaps significantly both with the forest and the field class. Strong spatial filtering could be used to obtain narrower and less overlapping distributions. This may prove to be effective, but at the price of reducing the spatial resolution. Another possibility could be to use a texture parameter to discriminate the urban areas. This also seems to have some potential, but again at the price of a reduction in the spatial resolution. We followed a most promising approach that exploits the interferometric capability of the sensors. In particular, long-term C-band coherence was considered to discriminate urban areas from other classes [28]. The expected effectiveness of this feature (which is significantly different from the Tandem coherence derived from ERS-1/2 images and used in standard approaches) depends on a higher temporal stability of the built up structures compared to most natural targets.

It is worth noting that long-term coherence and temporal variability are complementary, and are good candidates to separate the four land-cover classes, as shown in the qualitative signature diagram indicated in Fig. 2. In addition, they can be estimated from the same multitemporal datasets by using images acquired from the currently operating spaceborne SAR sensors. This is an important issue considering the operational applicability of the method and related data and processing costs.

Based on the analysis above, in the development of the feature-extraction module, we considered the *backscattering temporal variability* and *long-term coherence* information sources. The analytical description of the features computed to estimate this information is described in the following subsections.

B. Backscattering Temporal Variability Features

The estimation of the temporal variability of the backscattering coefficient is carried out starting from preprocessed images (see Section II). Different temporal variability estimators can be applied to the filtered backscatter images. Out of the six evaluated estimators (see Table I), we preferred the "standard

deviation of decibels values" for this study, because it is effective and because its values are more meaningful and easier to understand. It is defined as

$$\text{stdev} = \sqrt{\frac{1}{M}\cdot\sum_{i=1}^{M}(10\cdot\log_{10}\sigma_i)^2 - \left(\frac{1}{M}\cdot\sum_{i=1}^{M}10\cdot\log_{10}\sigma_i\right)^2}. \quad (2)$$

As an alternative to the temporal variability defined in (2), a temporal variability relative to a reference target can be calculated according to the following equation:

$$\text{stdev}_{\text{rel}} = \sqrt{\frac{1}{M}\cdot\sum_{i=1}^{M}\left(10\cdot\log_{10}\frac{\sigma_i}{\sigma_{\text{ref},i}}\right)^2 - \left(\frac{1}{M}\cdot\sum_{i=1}^{M}10\cdot\log_{10}\frac{\sigma_i}{\sigma_{\text{ref},i}}\right)^2} \quad (3)$$

where $\sigma_{\text{ref},i}$ is the estimate of the backscattering coefficient of the reference target in the image i. Both, the temporal variability defined in (2) and the temporal variability relative to a reference target defined in (3) are robust with respect to scene topography as the related radiometric factors are multiplicative. Thanks to this relative variability it is possible to reduce relative calibration errors (for instance, an offset of almost 0.5 dB between ERS-1 and ERS-2 based backscatter values was observed). The other advantage of relative variability compared to absolute variability is that large scale meteorological phenomena that have a significant effect on backscattering, such as freezing, are at least partially compensated. Of course, in this way more heterogeneous effects (as in the case of strong relief, depending on different temperatures at different elevations) cannot be taken into account. For the above reasons, in our case we used the standard deviation relative to selected reference forest areas within the image.

C. Long-Term Coherence Features

The development of SAR interferometry has recently proved that not only the amplitude of the radar signal, but also its phase contains valuable information for remote sensing applications. The interferometric phase (i.e., the phase difference between two images acquired from slightly different sensor positions) contains "geometric information," from which the three dimensional position of the scatter element can be derived. Estimation accuracy of the interferometric phase is characterized by the degree of coherence (generally referred to as coherence). Coherence is defined as the absolute value of the normalized complex correlation coefficient

$$|\gamma| = \left|\frac{\langle s_2\cdot s_1^*\rangle}{\sqrt{\langle s_1\cdot s_1^*\rangle\cdot\langle s_2\cdot s_2^*\rangle}}\right| \quad (4)$$

in which s_1 and s_2 denote the first and second complex SAR images respectively, and the brackets $\langle\rangle$ represent the ensemble average, which is estimated by spatial averaging. In our system, unlike in standard problems that utilize Tandem coherence, we focused our attention on the long term C-band coherence computed from images acquired 24 or 35 days apart (or multiples thereof). To compute long-term coherence, we recommend pairs of images with relatively short, perpendicular baseline components (<300 m). This is due to the fact that pairs of images with longer baselines tend to have low coherence also over urban areas. As confirmed by the preliminary experimental analysis shown in Fig. 3, separation of the urban class from other classes is rather good when the long-term coherence feature is used.

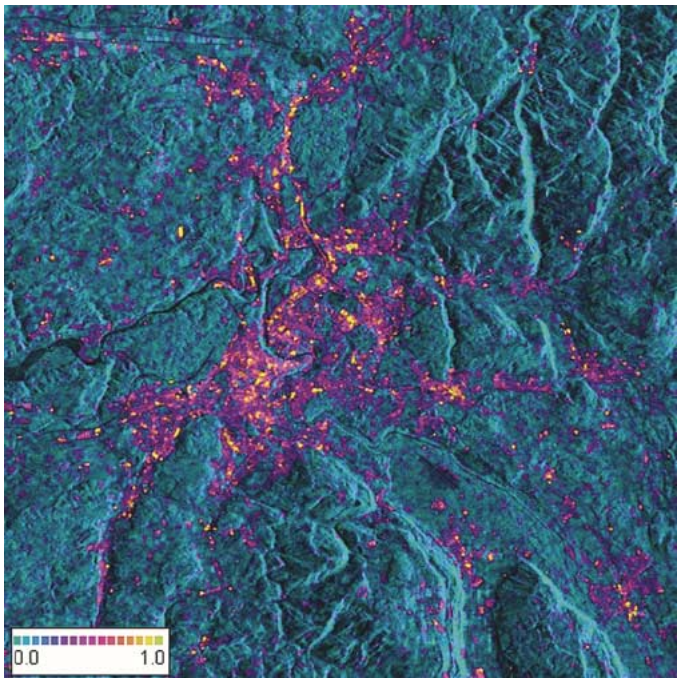

(a)

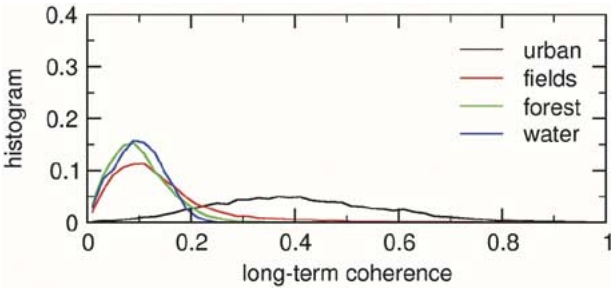

(b)

Fig. 3. Long-term coherence computed on a pair of ERS-2 images acquired 35 days apart with a baseline of 146 m. (a) Image showing the behavior of the long-term coherence parameter. (b) Histogram of the values of this parameter for the four investigated land-cover classes (area of the city of Bern, Switzerland).

IV. Proposed Classification Module Based on RBF Neural Networks

From a simple theoretical analysis, it is clear that the investigated multitemporal features have an irregular and complex joint probabilistic distribution, mainly because they are obtained by applying nonlinear operators to multitemporal SAR images. For this reason, parametric classification approaches (like Gaussian or Gamma distributed maximum likelihood algorithms) are not suited to our system, as it is impossible to formulate a reasonable model on class distributions in the considered feature space.

To overcome this difficulty and make the system more effective, we adopt distribution-free techniques that assume no

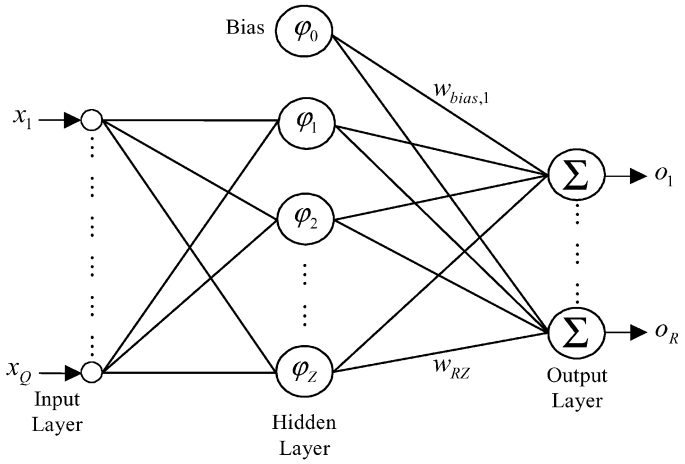

Fig. 4. Architecture of an RBF neural network classifier.

specific probabilistic models for class distributions. Among the possible nonparametric approaches, we did not consider rule-based hierarchical thresholding classifiers (as it often happens when multitemporal SAR images are available) [14], [21]. This is due to the fact that, although these approaches are simple and can also be applied to unsupervised classification problems, they rarely guarantee sufficiently high accuracies. As an alternative, we evaluated to use the k-nn technique. However, as extensively proved in the literature, this technique generally provides accuracies lower than or comparable with those exhibited by artificial neural networks, and it requires a higher computational time during the classification phase. For these reasons, we propose to use a classifier based on artificial neural networks that automatically fit the complexity of the different classes thanks to their nonlinear approximation properties and capability of learning from examples [29]. In the literature different models of neural networks have been proposed [11], [12], [29]. Among these, the multilayer perceptron (MLP) trained with the error backpropagation (EBP) learning algorithm is the most commonly used. However, MLPs exhibit drawbacks and limitations [12], [30], such as: the slow convergence of the EBP learning algorithm, the potential convergence to a local minimum, and the inability to detect that an input pattern has fallen in a region of the input space without training data. For these reasons, in our system we decided to use radial basis functions (RBF) neural network classifiers, which overcome some of the above problems by relying on a rapid training phase and by presenting systematic low responses to patterns that have fallen in regions of the input space with no training samples (this property is very important because it is strongly related to the capability of rejecting critical input samples) [31].

RBF neural networks are embedded in an architecture with an input layer, a single hidden layer characterized by units having activation functions $\varphi_z()$ with a radial symmetry (in this paper we consider Gaussian functions), and an output layer characterized by neurons with linear activation functions (see Fig. 4). In the most widely used classification architectures, the input layer is made up of as many units as the number of input features (i.e., Q), whereas the output layer contains as many neurons as the number of classes to be recognized (i.e., R). Each activation function $\varphi_z()$ associated with each unit of the hidden layer is characterized by a center vector $\bar{\mu}_z$ and a width h_z. Each output neuron o_l computes a weighted summation over the responses of the hidden neurons of the network for a given pattern $\bar{x}_p$, i.e.,

$$o_l(\bar{x}_p) = \sum_{z=1}^{Z} w_{lz} \cdot \varphi_z(\bar{x}_p) + w_{\text{bias},l} \tag{5}$$

where Z is the number of hidden neurons, w_{lz} represents the weight associated with the connection between the kernel function $\varphi_z()$ and the output neuron o_l, and $w_{\text{bias},l}$ is the bias of the output neuron o_l. Training of the RBF classifiers is usually carried out in two steps: 1) training of the hidden layer (i.e., selection of both the centers $\bar{\mu}_z$ and the width h_z of the kernel functions associated with the hidden units); 2) training of the output layer (i.e., the weights w_{lz} associated with the connections between the hidden and the output units are computed).

In training the hidden layer, in order to avoid the typical problems of standard learning procedures, the algorithm proposed in [31] was chosen. Such an algorithm, unlike traditional ones, considers the class membership of training samples to select the centers and widths of the kernel functions. In particular, it avoids the generation of mixed kernel functions and tunes the kernel widths to limit the overlapping in boundary regions between different classes. This results in: 1) an high stability of the classification accuracy versus the number of hidden neurons; 2) an high stability of the classification error versus the random initialization of the kernel centers during the training process; 3) a reduced computational time. These properties simplify the learning process of the classifier by significantly reducing the time devoted to the design of the network architecture.

The training of the output layer was carried out according to a standard procedure based on the minimization of a sum-of-squares error function carried out according to an algorithm based on the pseudoinverse matrix. It is worth noting that though RBF neural networks are made up of only one hidden layer, they can model the same complex mappings that multilayer perceptron neural networks model by means of multiple hidden layers.

V. Experimental Results

A. Description of the Test Area and Experiment Design

The test site considered in our experiments is related to an area around Bern, Switzerland. The area is rather complex, as it presents continuous alternation of all the different classes to be identified (i.e., fields, water, urban area, and forest). Moreover, since the selected area includes an irregular topography, it represents a challenging test case for SAR image analysis. A set of eight ERS complex SAR images, acquired between June 1995 and May 1996, was used for the investigation. An area of 20 km $\times$ 20 km was selected for the study. For validation purposes, a digital land use inventory and a Thematic Mapper image (acquired by the Landsat 5 satellite) were used. By analyzing these data, a set of regions of interest (ROIs) was defined [see Fig. 5(a) and (b)] from which the training and test sets (described

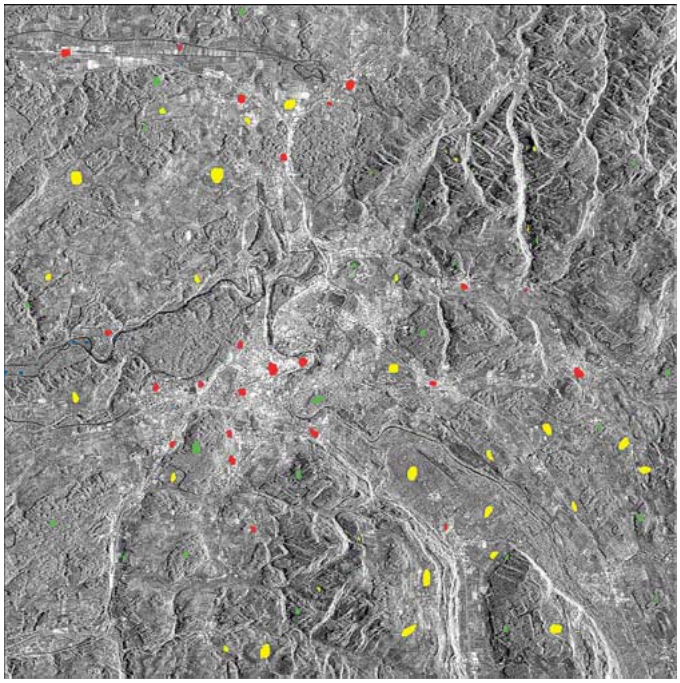

(a)

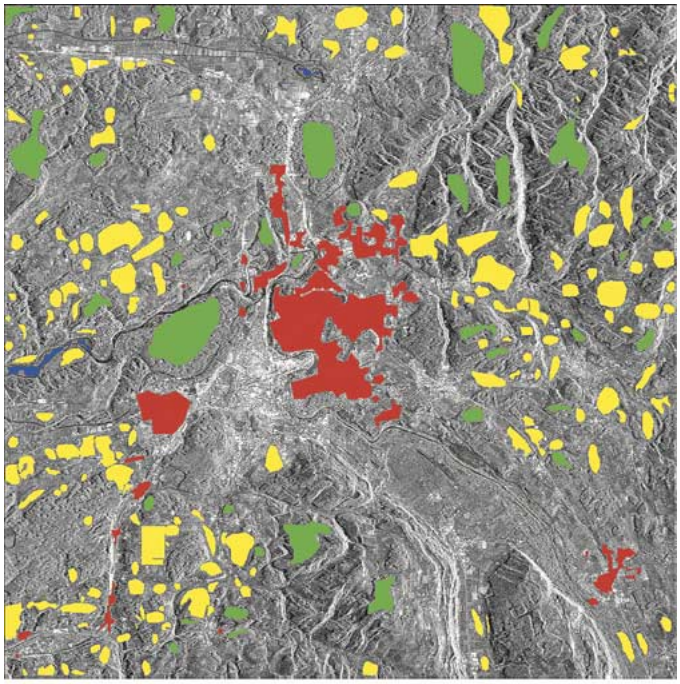

(b)

Fig. 5. Training and test sets overlapped to one of the eight ERS SAR images (four-class problem). (a) Training set. (b) Test set.

in Table II) were generated (the samples of the training and test sets were extracted from different ROIs). It is worth noting that most patterns were included in the test set to obtain a small-size training set with a number of samples comparable to the one that is typically available in operational applications of remote sensing image classification.

TABLE II
NUMBER OF TRAINING AND TEST SAMPLES USED IN THE EXPERIMENTS

Land-Cover Class	Training Set	Test Set
Forest	2130	35351
Urban Area	2198	34696
Water	450	1575
Fields	3804	67500
Total Pixels	8582	139122

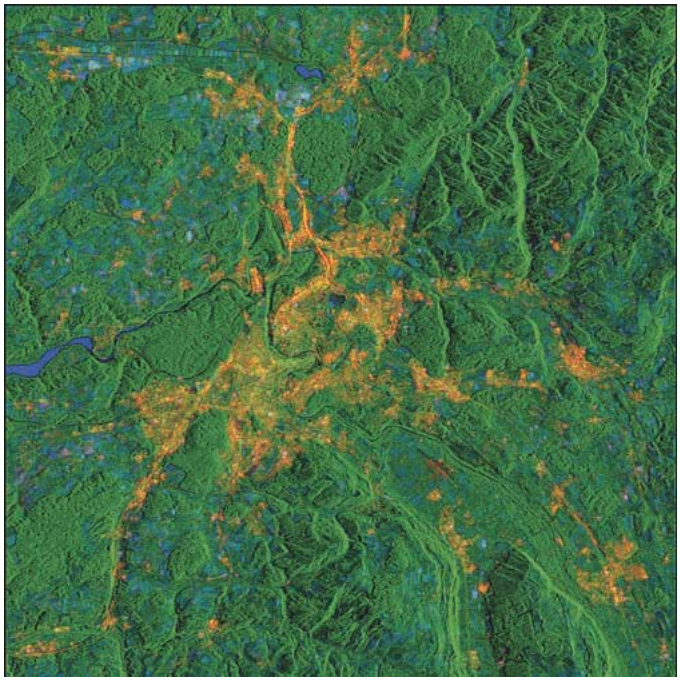

Fig. 6. RGB false-color composition of backscatter temporal variability, long-term coherence, and average backscattering coefficient (derived from the considered temporal series of eight ERS-1 SAR images acquired on the Bern area—Switzerland). This composition can be used for evaluating qualitatively the accuracies of the obtained classification maps.

As preprocessing, we applied radiometric calibration, coregistration to a common geometry in range-Doppler coordinates, and the temporal filtering described in Section II to all available images. We then selected four pairs of images, from which we generated four coherence images first (34/35 days time interval) and then an average image of them. Finally, the temporal variability feature was computed from the intensity images. Fig. 6 shows an RGB false-color composition of backscatter temporal variability, long-term coherence, and average backscattering coefficient, derived from the considered temporal series of eight ERS-1 SAR images.

In order to evaluate the effectiveness of the proposed system, several experiments were carried out. First, we focused our attention on the four-class classification problem (i.e., fields, water, urban area, and forest). We then applied the same process to discriminate only forest and nonforest areas. To better understand the behavior of the different modules of the proposed system, we carried out several trials generating three datasets on the basis of the aforementioned images and features: 1) a dataset with the eight temporally filtered images; 2) a

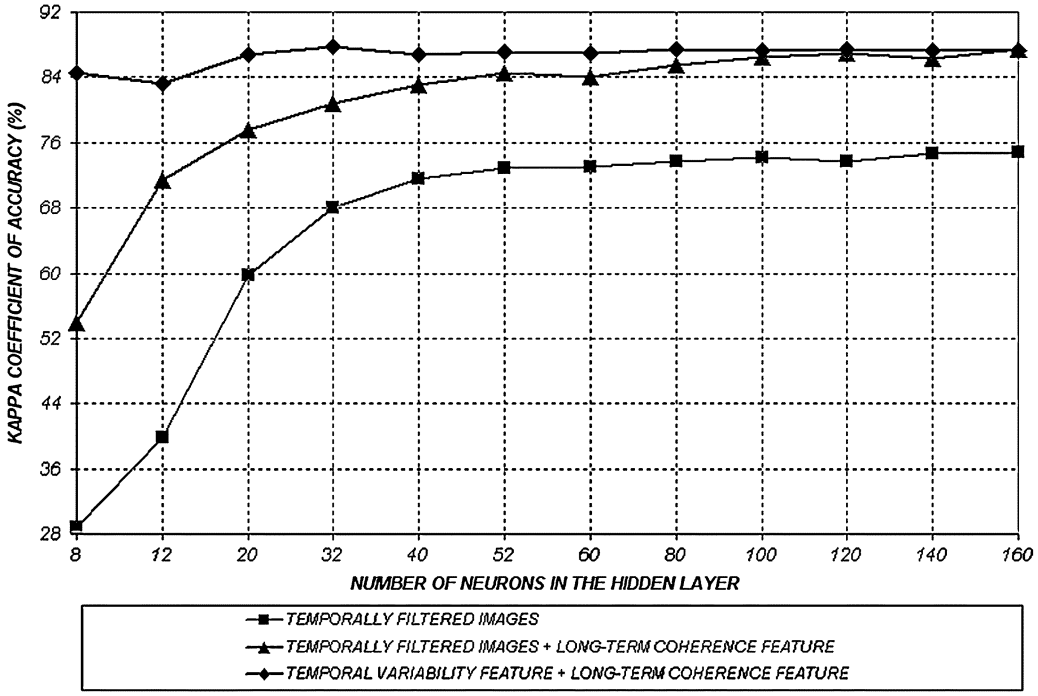

Fig. 7. Behavior of the Kappa coefficient of accuracy versus number of hidden neurons obtained with the three different sets of features considered (four-class problem).

dataset made up of the eight temporally filtered images plus the average long-term coherence image; and 3) a dataset with only the backscattering temporal variability feature (computed using the standard deviation of decibel values estimate with intensity scaling) and the average long-term coherence estimate.

After the training phase, we gave the patterns of the test set as input to the classifier, and for each trial we computed a confusion matrix and several accuracy statistics. Finally, the system was applied to the entire image to generate the global classification map. For all the statistics extracted from the confusion matrix (i.e., overall accuracy, user's and producer's accuracies, and Kappa coefficient of accuracy), we computed both the mean values and the standard deviations versus the number of hidden neurons, in order to assess the stability of the proposed classification system (in the paper we only report the most interesting results of this analysis). It is worth noting that producer's accuracy relates to omission errors, while user's accuracy indicates commission errors. The Kappa coefficient estimates the global accuracy of a classification process. It is widely used, because all the elements in the classification error matrix (not just the main diagonal) contribute to its computation.

As stated in Section IV, the RBF neural network classifier is made up of only three layers. The input layer has a number of neurons equal to the number of features of the used dataset. In our case, we considered datasets with eight, nine, and two features. Concerning the output layer, we defined as many units as the number of information classes (i.e., four neurons in the case of recognition of forest, water, fields, and urban classes, and two neurons in the classification of forest against nonforest). For each experiment, we carried out twelve trials, increasing the number of hidden neurons (and hence of activation functions) from 20 to 160. For the sake of simplicity, we chose an equal number of units for each information class. In this way, initially, we varied the neurons corresponding to each land-cover class from 5 to 40, in steps equal to 5. Successively, we made four additional trials with 2, 3, 8, and 13 neurons for each class, respectively, in order to better analyze the performances of the system when a low-complexity architecture is used.

B. Results for the Four-Class Problem

Let us first consider the results obtained in the four-class problem. Fig. 7 reports the behavior of the Kappa coefficient of accuracy versus the number of hidden neurons for the three considered datasets (made up of different features). As expected, the experiments carried out on the dataset containing the eight temporally filtered images had the worst accuracy, while the best accuracies were obtained with the dataset made up of only two features, i.e., the average long-term coherence and the backscattering temporal variability parameters. On analyzing the results in greater detail, we observe that for datasets with eight and nine features, the trend of the Kappa coefficient becomes stable only with a high number of neurons in the hidden layer (80–100 units). When few neurons are considered (two to five units per class), the outcomes are not satisfactory, especially for the first dataset (i.e., the percentage value of Kappa was lower than 60%). The average coherence feature proved to be very effective when added to the set of temporally filtered images, increasing the Kappa coefficient of accuracy by more than 15% with respect to the case with only temporally filtered images. This mainly depends on the effectiveness of the coherence to significantly reduce the confusion between both forest and urban areas and fields and urban areas. The dataset with the average coherence and the temporal variability features (which gave the highest accuracy) also exhibited a very interesting property: all accuracies grew steady and remained nearly constant on increasing the number

TABLE III
MEAN VALUES AND STANDARD DEVIATIONS OF KAPPA COEFFICIENTS OF ACCURACY (WITH RESPECT TO THE NUMBER OF HIDDEN NEURONS) YIELDED ON THE THREE INVESTIGATED FEATURE SETS (COMPUTED ON 12 TRIALS FOR EACH SET) BY THE PROPOSED RBF CLASSIFIER (FOUR-CLASS PROBLEM)

Feature Set	Mean Value of the Kappa Coefficient	Standard Deviation of the Kappa Coefficient
Temporally Filtered Images	65.42%	15.29
Temporally Filtered Images + Long-Term Coherence Feature	80.71%	9.60
Backscattering Temporal Variability Feature + Long-Term Coherence Feature	86.70%	1.38

TABLE IV
THRESHOLD VALUES APPLIED TO THE LONG-TERM COHERENCE AND TEMPORAL VARIABILITY FEATURES IN THE CLASSICAL HIERARCHICAL THRESHOLDING CLASSIFIER (FOUR-CLASS PROBLEM). THE THRESHOLDS ARE APPLIED TO THE PIXELS HIERARCHICALLY STARTING FROM THE FIRST ROW OF THE TABLE

Land-Cover Class	Range Between Threshold Values	
	Long-Term Coherence	Temporal Variability
Urban	0.2 - 1	0 - 1.3
Water	0 - 0.2	3 - 100
Forest	0 - 0.2	0 - 0.75
Fields	0 - 1	0 - 100

TABLE V
BEST OVERALL CLASSIFICATION ACCURACIES AND KAPPA COEFFICIENT OF ACCURACY EXHIBITED ON THE TEST SET BY THE PROPOSED RBF CLASSIFIER AND A STANDARD HIERARCHICAL THRESHOLDING CLASSIFIER (FOUR-CLASS PROBLEM)

Measure of Accuracy	Hierarchical Thresholding Classifier	Proposed RBF Neural Network Classifier
Overall Accuracy	86.15%	92.15%
Kappa Coefficient	78.13%	87.79%

of neurons in the hidden layer of the network. This stability was confirmed by the very low standard deviation value of the overall classification accuracy (versus the number of hidden units of the network) compared to the other two datasets (see Table III). Consequently, good results (similar to those yielded with a large number of hidden neurons with the previous set of features) were obtained using simple network architectures (i.e., less than eight neurons per class). This resulted in both very good classifier generalization capabilities (few parameters to estimate compared to more complex architectures) and a reduced computational time. It is worth noting that on this dataset the neural architecture with only 32 hidden neurons showed the best accuracy of all our trials.

In order to point out the improvements that can be obtained with the classification module defined in our system, we compared the results of the RBF architecture with those obtained when classifying the considered dataset with a hierarchical thresholding classifier (see [14] for a detailed description of this classifier). The different threshold values (see Table IV) used in this classifier were set on the basis of an experimental analysis carried out on the training data distribution. It is worth noting that the term "hierarchical" implies that the thresholds are

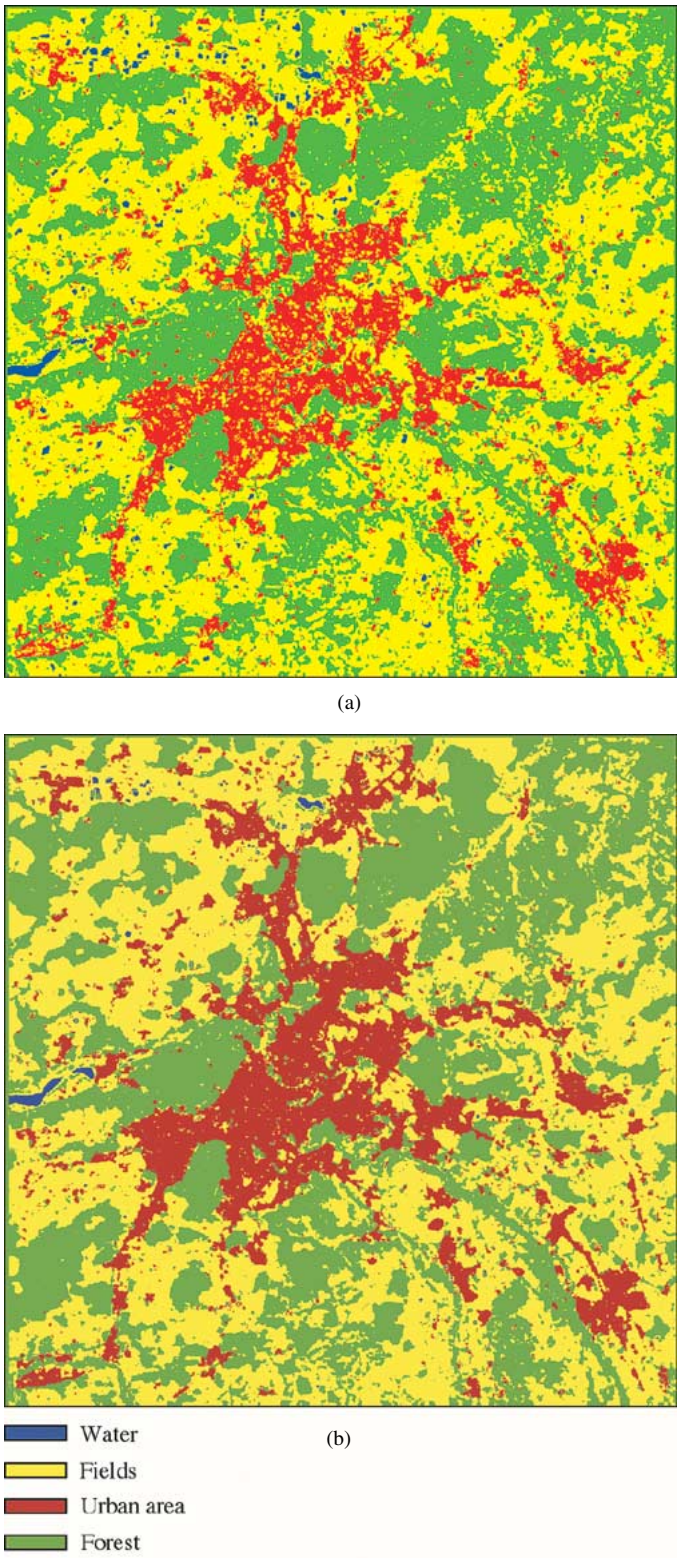

Fig. 8. Four-class classification problem using long-term coherence and temporal variability features. (a) Classification map obtained with a hierarchical thresholding classifier. (b) Classification map obtained with the most accurate RBF neural network classifier (architecture made up of 32 hidden neurons).

TABLE VI
CONFUSION MATRIX RESULTING FROM THE CLASSIFICATION OF THE TEST SET USING LONG-TERM COHERENCE AND BACKSCATTERING TEMPORAL VARIABILITY FEATURES WITH THE RBF NEURAL ARCHITECTURE THAT GAVE THE HIGHEST ACCURACY (I.E., 32 HIDDEN NEURONS)

Reference Data / Classified Data	Forest	Urban	Water	Fields	User's Accuracy
Forest	34345	673	135	2576	91.03%
Urban	129	31756	34	3670	89.23%
Water	0	75	1096	246	77.35%
Fields	877	2192	310	61008	94.75%
Producer's Accuracy	97.15%	91.53%	69.59%	90.38%	

TABLE VII
CONFUSION MATRIX RESULTING FROM THE CLASSIFICATION OF THE TEST SET USING LONG-TERM COHERENCE AND BACKSCATTERING TEMPORAL VARIABILITY FEATURES WITH THE HIERARCHICAL THRESHOLDING CLASSIFIER

Reference Data / Classified Data	Forest	Urban	Water	Fields	User's Accuracy
Forest	30286	554	0	2384	91.16%
Urban	1476	31872	19	6931	79.09%
Water	173	30	681	337	55.77%
Fields	3416	2240	875	57848	89.85%
Producer's Accuracy	85.67%	91.86%	43.24%	85.70%	

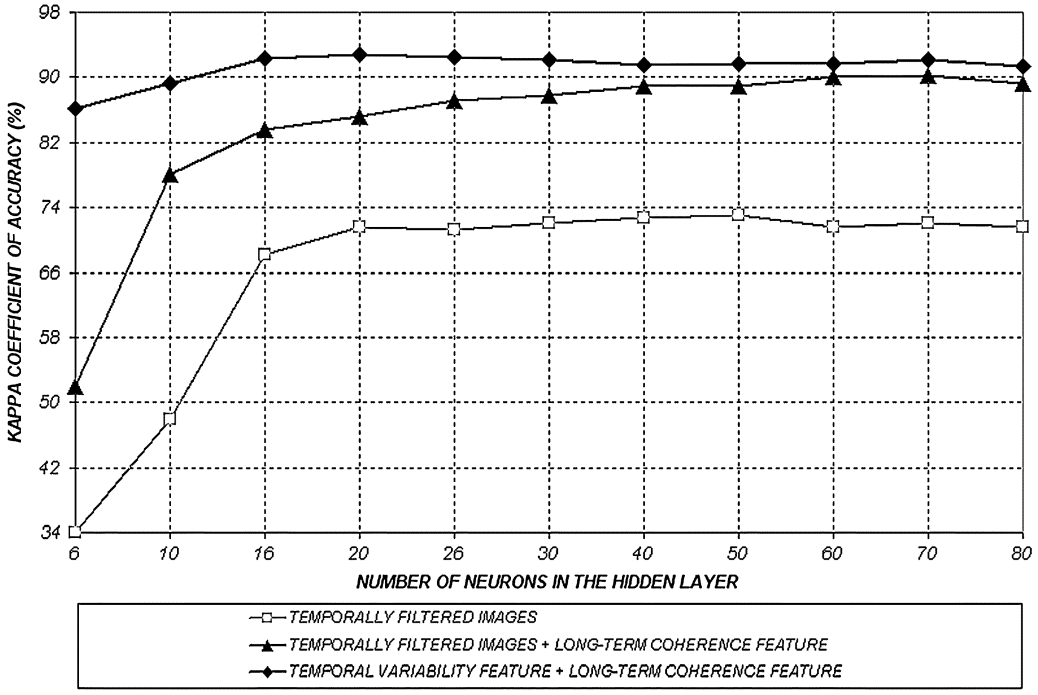

Fig. 9. Behavior of the Kappa coefficient of accuracy versus number of hidden neurons obtained with the three different sets of features considered (two-class forest against nonforest problem).

applied to the pixel hierarchically, starting form the first row of the Table IV (i.e., the condition of the first row is applied first, then the condition of the second row is applied for the remaining pixels, and so on). In all trials, we observed that the accuracies exhibited by the RBF neural network were always significantly higher than those obtained with the hierarchical thresholding classifier. From Table V, it can be seen that considering the best performances of the two classification methodologies, the proposed RBF neural network sharply increased (i.e., 6%) the overall accuracy compared to the thresholding approach. The significant improvement was stressed by the behavior of the Kappa coefficient of accuracy, which increased by about 10%. This behavior is also evident on comparing the classification maps provided by the two classifiers (see Fig. 8). In greater detail, the rule-based hierarchical thresholding classifier led to a number of problems that did not appear with the RBF neural network classifier: many fields were erroneously classified as water [see upper left corners of Fig. 8(a) and (b)], the edges of the forest areas were not always well shaped [see upper right corners of Fig. 8(a) and (b)], and the urban areas did not appear homogeneous and were confused with fields [see centers of Fig. 8(a) and (b)]. It is worth noting that from the analysis of the two classification maps, it seems that the gap of accuracy between the neural classifier and the hierarchical classifier is larger than that estimated on the test set. This is probably due to the fact that only few test samples were located in the most

TABLE VIII
MEAN VALUES AND STANDARD DEVIATIONS OF KAPPA COEFFICIENTS OF ACCURACY (WITH RESPECT TO THE NUMBER OF HIDDEN NEURONS) YIELDED ON THE THREE INVESTIGATED FEATURE SETS (COMPUTED ON 12 TRIALS FOR EACH SET) BY THE PROPOSED RBF CLASSIFIER (TWO-CLASS PROBLEM)

Feature Set	Mean Value of the Kappa Coefficient	Standard Deviation of the Kappa Coefficient
Temporally Filtered Images	66.02%	12.82
Temporally Filtered Images + Long-Term Coherence Feature	83.73%	11.11
Temporal Variability Feature + Long-Term Coherence Feature	91.24%	1.93

critical regions of the image (e.g., in border areas between classes), where the proposed neural classifier was far more accurate than the hierarchical approach.

For a better understanding of the results obtained, Tables VI and VII show the error matrices yielded by the two classifiers when using the temporal variability and the long term coherence features. When considering the RBF classifier, all accuracies are very high, except for the user accuracy of water (which is slightly lower than 70%). This undesired behavior of the water class depends on two main facts: it is a strongly minority class among the four considered, and it is confused with fields (which, like water, have low values of long-term coherence and high values of backscattering temporal variability). However, it is worth noting that the classification accuracy of the water class is 27% higher than the one obtained with a hierarchical classifier. In greater detail, on comparing Tables VI and VII, we observe that the results provided by the two classifiers are similar only in the producer's accuracy of urban areas and in the user's accuracy of forest areas, while the accuracies exhibited by the RBF neural classifier are significantly higher in all other cases.

C. Results for the Two-Class Problem

In the forest against nonforest classification, we used the same training and test sets of the four-class case, but the labels corresponding to water, fields, and urban areas were merged into the nonforest region of interest. It is worth noting that from the perspective of the classifier, this leads to a different problem (i.e., the decision regions are different as well as the model of the classification problem to be learnt from the classifiers). The architectures of the RBF classifier and the datasets were the same as for the previous trials.

Fig. 9 shows the behavior of the overall accuracy exhibited by the RBF neural classifier versus the number of hidden neurons for the different feature sets. From an analysis of the figure, it is easy to see that the results obtained here are very similar to those obtained in the four-class problem. In greater detail, also in this case the highest accuracy was obtained with the backscattering temporal variability and long-term coherence features (overall accuracy was always higher than 94% and the Kappa coefficient was higher than 86%), which was also confirmed to be very stable compared to the number of hidden neurons (starting from eight hidden units). Also for the two-class problem, the third feature set showed a very low standard deviation (see Table VIII). It is worth noting that, as expected, in all the trials carried out we obtained higher accuracies than in the four-class problem.

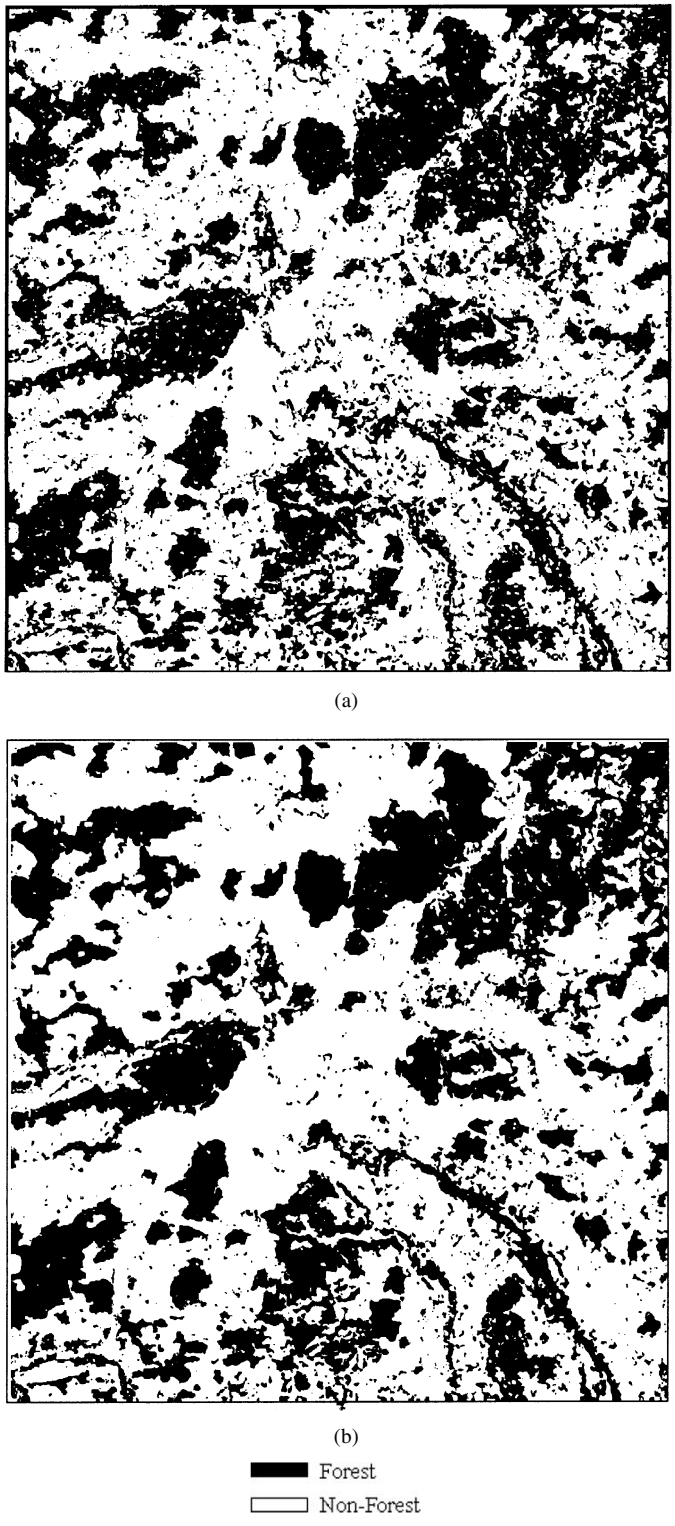

Fig. 10. Two-class classification problem using long-term coherence and temporal variability features. (a) Classification map obtained with a hierarchical thresholding classifier. (b) Classification map obtained with the most accurate RBF neural network classifier (architecture made up of 20 hidden neurons).

On analyzing the best accuracies provided by the considered classifiers (see Table IX), the improvements obtained using the RBF classifier compared to the rule-based hierarchic thresh-

TABLE IX
BEST OVERALL CLASSIFICATION ACCURACIES AND KAPPA COEFFICIENT OF ACCURACY EXHIBITED ON THE TEST SET BY THE PROPOSED RBF CLASSIFIER AND A STANDARD HIERARCHICAL THRESHOLDING CLASSIFIER (TWO-CLASS CASE)

Measure of Accuracy	Hierarchical Thresholding Classifier	Proposed RBF Neural Network Classifier
Overall Accuracy	93.95%	97.23%
Kappa Coefficient	84.46%	92.78%

olding classifier were confirmed significant: 3.3% for overall accuracy and 8.3% for the Kappa coefficient, respectively. On comparing the classification maps provided by the two classifiers (see Fig. 10), some very important differences can be observed. As in the four-class case, the hierarchical classifier led to several problems compared to the RBF neural network classifier: the edges of the woods in the hilly areas were not well shaped, especially in sites where the layover phenomenon is considerable [see upper left and lower right corners of Figs. 10(a) and (b)], some wide forest areas did not appear homogeneous [see left of Figs. 10(a) and (b)], and some urban areas were often wrongly classified as groves [see middle and right of Figs. 10(a) and (b)].

These results point out that the presented system (and in particular the proposed feature-extraction and classification modules) is a promising tool also for discriminating forest and nonforest areas in multitemporal SAR images.

VI. CONCLUSION

A system for the automatic classification of multitemporal SAR images has been proposed. The system was designed by integrating the features extracted on analyzing the physical properties of the multitemporal SAR signals with a pattern recognition approach. The resulting system is based on a standard set of preprocessing procedures, on a feature-extraction module, and on an RBF neural network classifier.

From an analysis of the results of all the experiments carried out using this system, we can conclude that it yielded both very high accuracies and very good stability compared to the parameter settings (e.g., number of units in the hidden layer of the neural architecture). In greater detail, we verified that: 1) the features of temporal variability of backscattering and long-term coherence are very effective in modeling the information present in a temporal series of SAR images (with respect to the land-cover classes considered in our experiments); and 2) RBF neural networks are a very effective classification methodology that allows to fully exploit the information in the two above features.

An important novelty of the proposed system consists of the combined use of temporal variability of backscattering and long-term coherence to discriminate several land-cover classes [in the literature, similar features have been used separately, for example, to discriminate between forest and agricultural fields (i.e., temporal variability of backscattering) or to separate urban areas from other areas (i.e., Tandem coherence)]. This is made possible by the use of a distribution-free RBF neural classifier. In this respect, a significant remark should be made as regards the relationship between the extracted features and the neural classifier. Thanks to the effectiveness of the extracted measures and to the properties of the classifier, it becomes possible to provide as input to the classification algorithm a significantly smaller number of parameters than the number of available multitemporal images, thus decreasing the complexity of the neural architecture and consequently increasing the generalization capabilities of the system. In addition, this leads to reduced computational costs, stable behavior of classification accuracy versus the number of hidden neurons of the classifier, and less critical constraints on the number of training samples necessary for an accurate and proper training of the classifier (it is well known that there is a direct proportionality link between the model complexity of the classifier, i.e., the number of parameters of the classifier, and the minimum number of per-class training samples that should be used to avoid poor generalization capability [32]).

The proposed system has been developed considering the forest, fields, urban, and water classes, and has been tested on two specific four-class and two-class problems. However, the methodology is general and can easily be extended to the discrimination of other classes, provided that multitemporal SAR images contain sufficient information for their separation and the feature extraction module is properly designed on the considered problem (as a future development of this work, we intend to extend the system to the discrimination between winter and summer field classes).

It is worth noting that the long-term coherence feature can be estimated from the same multitemporal data as the temporal variability of backscattering measure. In addition, the feature extraction methodology can be applied to currently operating spaceborne SAR sensors. This confirms the interest in the proposed system, which can be used to address classification applications with current available SAR data.

As a final remark, it is worth emphasizing that a joint approach to SAR data analysis that integrates an advanced pattern recognition methodology (based on machine learning techniques) with an accurate feature-extraction phase (based on the SAR-signal physics analysis) results in a system that outperforms the results obtained by applying these methodologies separately. This joint approach seems very promising to develop advanced operational tools for classifying multitemporal SAR data.

ACKNOWLEDGMENT

The authors wish to thank the anonymous reviewers for their constructive criticism.

REFERENCES

[1] C. J. Oliver and S. Quegan, *Understanding Synthetic Aperture Radar Images*. Norwood, MA: Artech House, 1998.

[2] E. Nezry, A. Lopes, D. Ducrot-Gambart, C. Nezry, and J. S. Lee, "Supervised classification of K-distributed SAR images of natural targets and probability of error estimation," *IEEE Trans. Geosci. Remote Sensing*, vol. 34, pp. 1233–1242, Sept. 1996.

[3] J. M. Durand, B. Gimonet, and J. Perbos, "SAR data filtering for classification," *IEEE Trans. Geosci. Remote Sensing*, vol. GE-25, pp. 629–637, 1987.
[4] Y. Dong, A. K. Milne, and B. C. Forster, "Segmentation and classification of vegetated areas using polarimetric SAR image data," *IEEE Trans. Geosci. Remote Sensing*, vol. 38, pp. 741–753, Mar. 2000.
[5] K. S. Chen, W. P. Huang, D. H. Tsay, and F. Amar, "Classification of multifrequency polarimetric SAR images using dynamic learning neural networks," *IEEE Trans. Geosci. Remote Sensing*, vol. 34, pp. 814–820, May 1996.
[6] L. E. Pierce, F. T. Ulaby, K. Sarabandi, and M. C. Dobson, "Knowledge-based classification of polarimetric SAR images," *IEEE Trans. Geosci. Remote Sensing*, vol. 32, pp. 1081–1086, Sept. 1994.
[7] Y. Hara, R. G. Atkins, S. H. Yueh, R. T. Shin, and J. A. Kong, "Application of neural networks to radar image classification," *IEEE Trans. Geosci. Remote Sensing*, vol. 32, pp. 100–109, Jan. 1994.
[8] M. C. Dobson, L. E. Pierce, and F. T. Ulaby, "Knowledge-based land-cover classification using ERS-1/J-ERS-1 SAR composites," *IEEE Trans. Geosci. Remote Sensing*, vol. 34, pp. 83–99, Jan. 1996.
[9] B. Solaiman, L. Pierce, and F. T. Ulaby, "Multisensor data fusion using fuzzy concepts: Application to land-cover classification using ERS-1/JERS-1 SAR composites," *IEEE Trans. Geosci. Remote Sensing*, vol. 37, pp. 1316–1326, May 1999.
[10] L. Bruzzone, D. F. Prieto, and S. B. Serpico, "A neural-statistical approach to multitemporal and multisource remote-sensing image classification," *IEEE Trans. Geosci. Remote Sensing*, vol. 37, pp. 1350–1359, May 1999.
[11] L. Bruzzone, F. Roli, and S. B. Serpico, "Structured neural networks for signal classification," *Signal Process.*, vol. 64, no. 3, pp. 271–290, Feb. 1998.
[12] S. B. Serpico, L. Bruzzone, and F. Roli, "An experimental comparison of neural and statistical nonparametric algorithms for supervised classification of remote-sensing images," *Pattern Recognit. Lett.*, vol. 17, no. 13, pp. 1331–1341, 1996.
[13] S. Quegan, T. Le Toan, J. J. Yu, F. Ribbes, and N. Floury, "Multitemporal ERS SAR analysis applied to forest mapping," *IEEE Trans. Remote Sensing*, vol. 38, pp. 741–753, Mar. 2000.
[14] U. Wegmüller, A. Wiesmann, T. Strozzi, and C. L. Werner, "Forest mapping with multitemporal SAR," in *Proc. ForestSAT'02 Conf.*, Edinburgh, U.K., Aug. 5–9, 2002.
[15] T. Le Toan, S. Quegan, M. Davidson, and J. M. Martinez, "Radar remote sensing of forests. Applications using existing satellite SAR data," in *Proc. 8th Int. Symp. Physical Measurements Signatures Remote Sensing*, 2001, pp. 33–40.
[16] K. Tansey, A. Luckman, and C. Schmullius, "Mapping boreal forest in Siberia with ERS SAR Interferometry," in *Proc. 25th Annu. Conf. Remote Sensing Society*, Cardiff, U.K., Sept. 8–10, 1999.
[17] T. Strozzi, P. B. G. Dammert, U. Wegmüller, J. M. Martinez, A. Beaudoin, J. Askne, and M. Hallikainen, "Landuse mapping with ERS SAR interferometry," *IEEE Trans. Geosci. Remote Sensing*, vol. 38, pp. 766–775, Feb. 2000.
[18] A. Luckman, J. Baker, and U. Wegmüller, "Repeat-pass interferometric coherence measurements of disturbed tropical forest from JERS and ERS satellites," *Remote Sens. Environ.*, vol. 73, pp. 350–360, 2000.
[19] T. Strozzi and U. Wegmüller, "Forest mapping with ERS SAR interferometry," in *Proc. 3rd ERS Scientific Symp.*, Florence, Italy, Mar. 17–20, 1997.
[20] W. Wagner, J. Vlietmeier, and C. Schmullius, "Information content of ERS SAR interferometric products for forest classification in Siberia, a case study over the Bolshemurtinskii forest enterprise," in *Proc. IGARSS*, Honolulu, HI, July 24–28, 2000.
[21] U. Wegmüller and C. L. Werner, "SAR interferometric signatures of forest," *IEEE Trans. Geosci. Remote Sensing*, vol. 33, pp. 1153–1161, Sept. 1995.
[22] ——, "Retrieval of vegetation parameters with SAR interferometry," *IEEE Trans. Geosci. Remote Sensing*, vol. 35, pp. 18–24, Jan. 1997.
[23] V. S. Frost and L. S. Yurovski, "Maximum likelihood classification of synthetic aperture radar imagery," *Comput. Vis., Graph., Image Process.*, no. 32, pp. 291–313, 1985.
[24] C. L. Werner, U. Wegmüller, T. Strozzi, and A. Wiesmann, "Gamma SAR and interferometric processing software," in *Proc. ERS-ENVISAT Symp.*, Gothenburg, Sweden, Oct. 16–20, 2000.
[25] R. Touzi, "A review of speckle filtering in the context of estimation theory," *IEEE Trans. Geosci. Remote Sensing*, vol. 40, pp. 2392–2404, Nov. 2002.
[26] S. Quegan and J. J. Yu, "Filtering of multichannel SAR images," *IEEE Trans Geosci. Remote Sensing*, vol. 39, Nov. 2001.
[27] V. S. Frost, J. A. Stiles, K. S. Shanmugan, and J. C. Holtzman, "A model for radar images and its application to adaptive digital filtering of multiplicative noise," *IEEE Trans. Pattern Anal. Machine Intell.*, vol. PAMI-4, pp. 157–166, Mar. 1982.
[28] T. Strozzi and U. Wegmüller, "Delimitation of urban areas with SAR interferometry," in *Proc. IGARSS*, Seattle, WA, July 6–10, 1998.
[29] J. A. Benediktsson, P. H. Swain, and O. K. Ersoy, "Neural network approaches versus statistical methods in classification of multisource remote sensing data," *IEEE Trans. Geosci. Remote Sensing*, vol. 28, pp. 540–552, July 1990.
[30] L. Bruzzone and S. B. Serpico, "Classification of imbalanced remote-sensing data by neural networks," *Pattern Recognit. Lett.*, vol. 18, no. 11–13, pp. 1323–1328, 1997.
[31] L. Bruzzone and D. F. Prieto, "A technique for the selection of kernel-function parameters in RBF neural networks for classification of remote-sensing images," *IEEE Trans. Geosci. Remote Sensing*, vol. 37, pp. 1179–1184, Mar. 1999.
[32] C. M. Bishop, *Neural Networks for Pattern Recognition*. Oxford, U.K.: Clarendon Press, 1995.

Lorenzo Bruzzone (S'95–M'99–SM'03) received the laurea (M.S.) degree in electronic engineering (summa cum laude) and the Ph.D. degree in telecommunications, both from the University of Genoa, Genoa, Italy, in 1993 and 1998, respectively.

He is currently Head of the Remote Sensing Laboratory in the Department of Information and Communication Technologies at the University of Trento, Trento, Italy. From 1998 to 2000, he was a Postdoctoral Researcher at the University of Genoa. From 2000 to 2001, he was an Assistant Professor at the University of Trento, where he has been an Associate Professor of telecommunications since November 2001. He currently teaches remote sensing, pattern recognition, and electrical communications. His current research interests are in the area of remote sensing image processing and recognition (analysis of multitemporal data, feature selection, classification, data fusion, and neural networks). He conducts and supervises research on these topics within the frameworks of several national and international projects. He is the author (or coauthor) of more than 100 scientific publications, including journals, book chapters, and conference proceedings. He is a referee for many international journals and has served on the Scientific Committees of several international conferences.

Dr. Bruzzone ranked first place in the Student Prize Paper Competition of the 1998 IEEE International Geoscience and Remote Sensing Symposium (Seattle, July 1998). He is the Delegate in the scientific board for the University of Trento of the Italian Consortium for Telecommunications (CNIT) and a member of the Scientific Committee of the India–Italy Center for Advanced Research. He was a recipient of the *Recognition of IEEE Transactions on Geoscience and Remote Sensing Best Reviewers* in 1999 and was a Guest Editor of a Special Issue of the IEEE TRANSACTIONS ON GEOSCIENCE AND REMOTE SENSING on the subject of the analysis of multitemporal remote sensing images (November 2003). He was the General Co-chair of the First and Second IEEE International Workshop on the Analysis of Multi-temporal Remote-Sensing Images (Trento, Italy, September 2001—Ispra, Italy, July 2003). Since 2003, he has been the Chair of the SPIE Conference on Image and Signal Processing for Remote Sensing (Barcelona, Spain, September 2003—Maspalomas, Gran Canaria, September 2004). He is an Associate Editor of the IEEE GEOSCIENCE AND REMOTE SENSING LETTERS. He is a member of the International Association for Pattern Recognition (IAPR) and of the Italian Association for Remote Sensing (AIT).

Mattia Marconcini was born in Verona, Italy, in 1980. He received the "first level laurea" (B.A.) degree in telecommunications engineering (summa cum laude) from the University of Trento, Trento, Italy, in 2002. His thesis was on classification of multitemporal SAR images. He is currently attending the "laurea specialistica" course (M.S.) in telecommunication engineering at the University of Trento.

His main interests are in the area of remote sensing image processing and recognition. In particular, his interests are in neural networks for classification purpose and radar image processing.

Urs Wegmüller (M'94–SM'03) received the M.S. and Ph.D. degrees from the University of Bern, Bern, Switzerland, in 1986 and 1990, respectively, both in physics.

Between 1991 and 1992, he was a Visiting Scientist at the Jet Propulsion Laboratory, California University of Technology, Pasadena, working on the retrieval of canopy parameters from microwave remote sensing data. Between 1993 and 1995, at the University of Zürich, Zürich, Switzerland, his research included interferometric data processing, theoretical modeling of scattering in forest canopies, and retrieval algorithm development for geo- and biophysical parameters using SAR interferometry. In 1995, he was a founding member of GAMMA Remote Sensing AG, Muri, Switzerland, which is active in the development of signal processing techniques and remote sensing applications. As CEO of GAMMA, he has overall responsibility for GAMMA's activities. In addition, he is directly responsible for a number of research and commercial projects of GAMMA. His main involvement currently is in the development of applications and the definition and implementation of related services in land surface deformation mapping, hazard mapping, landuse mapping, and topographic mapping. He is Principal Investigator for ERS, ENVISAT, SRTM, and ALOS announcement of opportunity projects on SAR and SAR interferometry-related calibration issues, application development, and demonstration.

Andreas Wiesmann (M'00) received the M.S. degree in physics and the Ph.D. degree in natural sciences, both from the University of Bern, Bern, Switzerland, in 1994 and 1998, respectively.

In 1998, he joined Gamma Remote Sensing AG, Muri, Switzerland, as a Senior Research Scientist. His current work includes the development of SAR- and InSAR-based applications for earth observation.